Ilya V. Veksler · Yana M. Fedorchuk
Troels F.D. Nielsen

# Phase equilibria in the silica-undersaturated part of the KAlSiO$_4$ – Mg$_2$SiO$_4$ – Ca$_2$SiO$_4$ – SiO$_2$ – F system at 1 atm and the larnite-normative trend of melt evolution

**Abstract** The evolution of nephelinitic melts in equilibrium with mica-bearing liquidus assemblages and melting relations have been studied on two silica-undersaturated joins of the KAlSiO$_4$ – Mg$_2$SiO$_4$ – Ca$_2$SiO$_4$ – SiO$_2$ – F system at atmospheric pressure by quench runs in sealed platinum capsules. Fluorine has been added to the batch compositions by the direct exchange of fluorine for oxygen ($2F^- = O^{2-}$). The first join is the pseudo-ternary Forsterite – Diopside – KAlSiO$_3$F$_2$ system. Forsterite, diopside, F-phlogopite and leucite crystallisation fields and a fluoride-silicate liquid immiscibility solvus are present on the liquidus surface of the join. Sub-liquidus and sub-solidus phases include akermanite, cuspidine, spinel, fluorite and some other minor fluorine phases. The second system is the pseudo-binary Akermanite – F-phlogopite join that intersects the Forsterite – Diopside – KAlSiO$_3$F$_2$ join. Akermanite, forsterite, diopside, F-phlogopite, leucite and cuspidine are found to crystallise on the join. Forsterite (fo) and leucite (lc) are related to F-phlogopite (phl) by a reaction with the fluorine-bearing liquid: fo + lc + l = phl, and the reaction proceeds until forsterite or leucite are completely consumed. The reaction temperature and resulting phase association depend on batch composition. Thus, leucite is not stable in the sub-solidus of the Akermanite – F-phlogopite join, but is preserved in a part of the Forsterite – Diopside – KAlSiO$_3$F$_2$ system where forsterite reacts out, or does not crystallise at all. The phlogopite-in reaction has an important effect on the composition of the coexisting liquid. The liquids initially saturated in forsterite evolve to extremely Ca rich, larnite-normative residuals. The experimental data show that larnite-normative melilitolites can crystallise from evolved melilititic melts generated from "normal" melanephelinitic parental magmas *with no normative larnite*. The evolution towards melilitites requires fractionation of phlogopite-bearing assemblages under volatile pressure.

## Introduction

The experimental study is designed to model the effect of volatiles on the crystal fractionation path in ultramafic alkaline magmatic systems at low pressure. Of special interest is the link between the stability of liquidus phlogopite and the development of highly larnite normative melilitite melts. We have focused on phlogopite because it is the most abundant hydrous liquidus phase in ultramafic alkaline rocks. Phlogopite is common not only in potassic rocks, but also in plutonic complexes of sodium-rich ultramafic alkaline rocks and related carbonatites. In both K- and Na-rich systems it is often found in close association with melilite in Ca-rich melilitic rocks. In a study of the petrography and bulk chemical composition of alkaline dyke swarms in the Gardiner complex, Nielsen (1994) suggested that highly larnite normative melilitolites may form from late-stage residual melts by phlogopite, amphibole, clinopyroxene and Fe-Ti oxide fractionation from a melanephelinite parental melt under closed, volatile-rich conditions in shallow-level magma chambers.

Phlogopite crystallisation has previously been studied mainly in the Ca-free KAlSiO$_4$ – Mg$_2$SiO$_4$ – SiO$_2$ – H$_2$O(F) system (Luth 1967; Modreski and Boettcher 1973; Wendlandt and Eggler 1980 a, b; Foley et al. 1986; Gupta and Green 1988; Melzer and Foley 1996). Melilite liquidus equilibria have mostly been studied at atmospheric pressure in dry systems, such as NCMAS (Pan

I.V. Veksler (✉)[1] · Y.M. Fedorchuk
Vernadsky Institute of Geochemistry and Analytical Chemistry, Kosygin str., 19, Moscow 117975, Russia

T.F.D. Nielsen
Geological Survey of Denmark and Greenland, Thoraves 8, DK-2400 Copenhagen K and Danish Lithosphere Centre, Øster Voldgade, 10, DK-1350 Copenhagen, Denmark

*Present address*:
[1]Danish Lithosphere Centre, Øster Voldgade 10, DK-1350 Copenhagen, Denmark
E-mail: ivv@dlc.ku.dk

Editorial responsibility: J. Hoefs

and Longhi 1989, 1990; Soulard et al. 1992), from which phlogopite is absent. High-pressure melting experiments with phlogopite-bearing potassic rocks were reviewed by Edgar and Vukadinovic (1992) and Foley (1992). In most cases, however, compositions of glasses in run products were not analysed due to problems with quench phlogopite. The aim of this study is accordingly to obtain experimental data on phlogopite-melilite liquidus relationships at crustal pressures, which have not previously been documented experimentally and to investigate the suggested evolution towards larnite-normative residual melt composition in phlogopite-bearing systems at low pressure. For this purpose we have studied several joins in the silica-undersaturated part of the $KAlSiO_4$ – $Mg_2SiO_4$ – $Ca_2SiO_4$ – $SiO_2$ system, known as the kalsilite-based normative tetrahedron (Yoder 1986) with the addition of fluorine.

The kalsilite-based normative tetrahedron (Fig. 1) has long proved to be a useful model for the study and the graphic presentation of phase equilibria in potassium-rich igneous rocks. The system, however, has
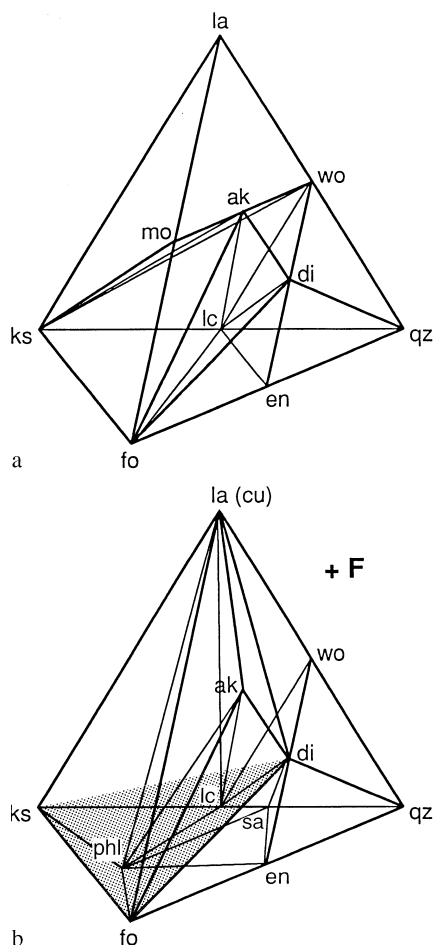


Fig. 1a, b Kalsilite-based normative tetrahedron. **a** volatile-free low-pressure conditions (Yoder 1986); **b** low-pressure fluorine-doped system at the conditions of phlogopite and cuspidine stability. *Shaded triangle* shows the $Mg_2SiO_4$ – $CaMgSi_2O_6$ – $KAlSiO_3F_2$ pseudoternary join. See the Appendix for abbreviations

broader application. The addition of water to the components of the tetrahedron at pressures $> 0.7$ kbar allows the study of the phlogopite-bearing phase assemblages. Phlogopite is a key phase in many petrological models, as it is the main reservoir for potassium, $H_2O$ and a number of trace elements in the lithospheric mantle. Thus, studies of partial melts of phlogopite-bearing mantle assemblages at elevated pressures are a necessity for understanding the origin of a broad spectrum of mantle-derived magmas. On the other hand, the crystallisation of liquidus phlogopite in shallow-level magma chambers at lower pressure may, as suggested by Nielsen (1994), have fundamental effect upon the crystal fractionation path of magmatic systems and result in the diversity of plutonic and volcanic rocks of ultramafic alkaline complexes.

Liquidus phlogopite can be stabilised in the kalsilite-based normative tetrahedron in two ways: (1) by applying water pressure $> 0.7$ kbar; or (2) by adding fluorine by substitution of fluorine for oxygen ($2F^- = O^{2-}$). We have chosen the latter method because fluorine-doped runs may be performed at 1 atm in sealed platinum capsules and such runs provide: (1) higher quenching rates; (2) the possibility to avoid quench phlogopite; (3) the formation of homogeneous glasses suitable for microprobe analyses. A further important point is that F-phlogopite thermal stability exceeds that of the OH-analogue by about 200 °C (Shell and Ivey 1969; Munoz 1984). The F-doped system thus enables the study of the extreme case of maximum phlogopite stability and its maximum effect on melt evolution.

## Previous studies

Anhydrous phase equilibria in the kalsilite-based normative basalt tetrahedron at atmospheric pressure have been studied in detail for several decades (e.g. Schairer and Bowen 1938; Luth 1967; Gupta 1972). Experimental results on phase equilibria in the tetrahedron at anhydrous conditions and under $H_2O$ pressure are reviewed by Yoder (1986) who showed that phlogopite takes part in a number of heteromorphic reactions and has an important effect on the topology of subtetrahedra within the kalsilite-based normative tetrahedron (Fig. 1).

Experimental studies at high pressure concentrated on the kalsilite-forsterite-quartz ($KAlSiO_4$ – $Mg_2SiO_4$ – $SiO_2$) border join. Phase relationships for this join have been investigated at different *P-T* conditions and in the presence of several volatile components: $H_2O$, $CO_2$, F (Luth 1967; Modreski and Boettcher 1973; Wendlandt and Eggler 1980a, b; Wendlandt 1984; Foley et al. 1986; Gupta and Green 1988). Much attention has been paid to the position of the fo + l = en + phl reaction point, where liquid is in equilibrium with the phase assemblage similar to that of the phlogopite-bearing upper mantle. Effects of fluorine on the phase equilibria in the kalsilite-forsterite-quartz system have been studied by Foley et al. (1986) and Melzer and Foley (1996). These

investigations showed that the phlogopite liquidus field greatly expands with increasing fluorine content in the system.

A few high-pressure experiments have been carried out with Ca-bearing compositions. These include 1:1 (weight) diopside–phlogopite mixture (Kushiro 1970; Modreski and Boettcher 1973) in which the clinopyroxene–phlogopite association has been shown to be stable at pressures up to at least 32 kbar.

## Experimental and analytical methods

The starting materials for the runs are mixtures of synthetic forsterite, diopside, akermanite, potassium aluminosilicate glass and chemical-grade $AlF_3$ (for the $Mg_2SiO_4 - CaMgSi_2O_6 - KAlSiO_3F_2$ join), or $MgF_2$ (for the $Ca_2MgSi_2O_7 - KMg_3AlSi_3O_{10}F_2$ join). Synthetic minerals and glasses were prepared from pure oxides and carbonates ($SiO_2$, $Al_2O_3$, $MgO$, $CaCO_3$, $K_2CO_3$) by mixing of appropriate proportions in a mortar under acetone and sintering in air at 950–1000 °C. Sintered mixtures were then crushed and heated again to temperatures between 1100 to 1400 °C, depending on the compound. Ready to use charges were kept dry in a desiccator. However, peralkaline glasses and some fluoride compounds used in reactant mixtures are hygroscopic and presence of some water in our charges can not be ruled out completely.

Quench experiments were carried out at 1 atm in a vertical electric furnace with a heater made of platinum wire. About 20 mg of fine powder were sealed in platinum capsules. The capsules were weighted before and after the runs to check for seal failure and fluorine loss. The temperature was controlled by Pt/PtRh30 thermocouple calibrated against the melting point of gold. The accuracy of temperature measurements is estimated to be ±5 °C.

Run durations varied from 5 to 75 hours depending on the temperature and composition of the mixtures (see Table 1). We used two different heating procedures to check for equilibrium. In the majority of the runs starting mixtures were overheated up to about 100 °C above the run temperature and then slowly cooled to the run conditions. In high-temperature runs (>1200 °C) and in a few control runs at lower temperatures the run conditions were directly attained without overheating. Control runs show that the phase compositions of the run products are independent of the heating procedure. Nevertheless, runs with overheating usually produce larger crystals (above 10 microns) that are better suited for optical identification and electron microprobe studies. The samples were quenched in cold water. Mostly, quench rates were sufficiently high to avoid quench phlogopite and to produce homogeneous transparent glass.

Run products were studied optically in index oil. Crystal phases in some samples were determined by X-ray diffraction. Chemical compositions of crystal phases and glasses in selected samples were analysed by JEOL 7 Superprobe electron microprobe, Department of Geology, University of Copenhagen as described by Nielsen et al. (1997). A defocused beam (beam size 15–20 μm) was used for analyses of glasses to reduce K and F-loss. Crystallised globules of immiscible fluoride liquid were analysed by scanning method.

## Experimental results

Four F-doped joins in the kalsilite tetrahedron were studied and include: the Forsterite – $KAlSiO_3F_2$ join, the Diopside – $KAlSiO_3F_2$ join, the Forsterite – Diopside – $KAlSiO_3F_2$ join and the Akermanite – F-Phlogopite join. Run conditions and phase composition of the run products are listed in Table 1. Liquidus surface projection for the $Mg_2SiO_4 - CaMgSi_2O_6 - KAlSiO_3F_2$ join is presented in Fig. 2. The $T$-$x$ phase diagrams for the $Ca_2MgSi_2O_7 - KMg_3AlSi_3O_{10}F_2$ and the $CaMgSi_2O_6 - KAlSiO_3F_2$ joins are shown in Figs. 3 and 4. Nine crystalline phases were identified in the run products: forsterite, diopside, leucite, akermanite, F-phlogopite, spinel, cuspidine, fluorite, and F-chondrodite (?). Some aluminofluorides (presumably $K_3AlF_6$) may be also present in F-rich compositions. Besides the crystalline phases, immiscible fluoride liquid is observed in the F-rich part of the $Mg_2SiO_4 - CaMgSi_2O_6 - KAlSiO_3F_2$ join (see Figs. 2 and 4). A vapour phase, though omitted in Table 1, may occur. Tiny (5–10 μm) gas-filled vesicles are seen in some run products. They may suggest the presence of a free vapour phase during the runs, or a vapour phase formed during the quenching. In all cases, however, there is no indication (within the error of EMP analyses) of significant F-loss to a free vapour phase.

## Crystalline phases

### Forsterite

Forsterite forms small (5–10 μm) euhedral prismatic crystals and rounded oval grains. In the index oil it can in general be distinguished from diopside by smaller grain size and with confidence by parallel extinction. Analyses show that forsterite has nearly constant stoichiometric composition close to the ideal formula. The CaO content is 0.27–2.29 wt%.

### Diopside

Clinopyroxene which, according to EMP data (Table 2), is close to pure diopside, usually occurs in the run products as large (about 40–50 μm) elongated prismatic crystals. Representative EMP analyses in Table 2 show that Al substitutes for some Si in tetrahedral sites of clinopyroxene structure. This substitution is charge-balanced mainly by $Al^{3+}$-$Mg^{2+}$ exchange in M1 octahedral sites.

### Leucite

High-temperature liquidus leucite occurs as medium-size (20–30 μm) perfect tetragontrioctahedral crystals. At lower temperatures it forms irregular grains. Oval glass inclusions are common in leucite. Under crossed nicols leucite is usually isotropic, but in some crystals complex twinning structures can be observed. The composition of leucite is stable and very close to the ideal formula. The CaO content does not exceed 0.22 wt%. Magnesium is also present in small amounts (0.07–0.23 wt% MgO) and appears to substitute for aluminium and silicon in tetrahedral sites.

**Table 1** Run conditions and run products. Abbreviations for components and phases are listed in the Appendix

| Sample | Starting composition, wt% | Duration, h | $T$ °C | Phase composition of run products |
|---|---|---|---|---|
| 1 | 2 | 3 | 4 | 5 |
| Forsterite – KAlSiO$_3$F$_2$ join | | | | |
| FKF-63 | Fo80:KF20 | 5 | 1350 | l + fo |
| FKF-74 | | 7.5 | 1300 | l + fo + phl |
| FKF-48 | | 6.5 | 1250 | l + fo + phl |
| FKF-17 | | 55 | 1200 | l + fo + phl + sp |
| FKF-1 | | 75 | 1150 | fo + phl fine-grain aggregate |
| FKF-32 | | 60 | 1100 | fo + phl fine-grain aggregate |
| FKF-64 | Fo60:KF40 | 5 | 1350 | l + fo + phl |
| FKF-75 | | 7.5 | 1300 | l + fo + phl |
| FKF-49 | | 6.5 | 1250 | l + fo + phl + sp |
| FKF-18 | | 55 | 1200 | l + fo + phl + sp |
| FKF-2 | | 75 | 1150 | fo + phl fine-grain aggregate |
| FKF-33 | | 60 | 1100 | fo + phl + hu? fine-grain |
| FKF-65 | Fo40:KF60 | 5 | 1350 | l + fo + phl |
| FKF-76 | | 7.5 | 1300 | l + fo + phl |
| FKF-50 | | 6.5 | 1250 | l + fo + phl |
| FKF-19 | | 55 | 1200 | l + fo + phl |
| FKF-3 | | 75 | 1150 | l + fo + phl |
| FKF-34 | | 60 | 1100 | l + fo + phl |
| FKF-85 | Fo30:KF70 | 7 | 1216 | l + phl |
| FKF-110 | | 7 | 1130 | l + phl |
| FKF-77 | Fo20:KF80 | 7.5 | 1300 | l |
| FKF-51 | | 6.5 | 1250 | l + phl |
| FKF-20 | | 55 | 1200 | l + phl |
| FKF-35 | | 60 | 1100 | l + phl |
| FKF-95 | | 18 | 1050 | l + phl |
| FKF-86 | Fo90:KF10 | 7 | 1216 | l |
| FKF-96 | | 18 | 1050 | l + phl |
| FKF-120 | | 53 | 993 | l + phl |
| KF-143 | KF | 24 | 850 | l |
| KF-144 | | 24 | 650 | l + few dendritic rystals |
| KF-145 | | 24 | 650 | l + rare crystals |
| Diopside – KAlSiO$_3$F$_2$ join | | | | |
| DKF-87 | Di80:KF20 | 7 | 1216 | l |
| DKF-21 | | 55 | 1200 | l + di |
| DKF-5 | | 75 | 1150 | l + di + lc |
| DKF-111 | | 7 | 1130 | l + di + lc |
| DKF-36 | | 60 | 1100 | l + di + lc + traces phl |
| DKF-97 | | 18 | 1050 | l + di + lc + phl |
| DKF-53 | Di60:KF40 | 6.5 | 1250 | l |
| DKF-88 | | 7 | 1216 | l + lc |
| DKF-22 | | 55 | 1200 | l + lc + traces phl |
| DKF-112 | | 7 | 1130 | l + lc + phl |
| DKF-37 | | 60 | 1100 | l + lc + phl + di |
| DKF-98 | | 18 | 1050 | l + lc + phl + di |
| DKF-121 | | 53 | 993 | lc + phl + di + fl |
| DKF-146 | Di50:KF50 | 5 | 1170 | l + lc |
| DKF-54 | Di40:KF60 | 6.5 | 1250 | l |
| DKF-89 | | 7 | 1216 | l$_s$ + l$_f$ |
| DKF-23 | | 55 | 1200 | l$_s$ + l$_f$ + lc |
| DKF-113 | | 7 | 1130 | l$_s$ + l$_f$ + lc + phl |
| DKF-38 | | 60 | 1100 | l$_s$ + l$_f$ + lc + phl |
| DKF-99 | | 18 | 1050 | l$_s$ + l$_f$ + lc + phl |
| DKF-122 | | 53 | 993 | l$_s$ + l$_f$ + lc + phl |
| DKF-133 | | 50 | 950 | l + lc + phl + fl |
| DKF-78 | Di20:KF80 | 7.5 | 1300 | l |
| DKF-55 | | 6.5 | 1250 | l$_s$ + l$_f$ |
| DKF-24 | | 55 | 1200 | l$_s$ + l$_f$ |
| DKF-39 | | 60 | 1100 | l$_s$ + l$_f$ |
| DKF-100 | | 18 | 1050 | l$_s$ + l$_f$ + phl |
| DKF-123 | | 53 | 993 | l$_s$ + l$_f$ + phl |
| DKF-134 | | 50 | 950 | l$_s$ + l$_f$ + phl + lc |
| Forsterite – diopside – KAlSiO$_3$F$_2$ join | | | | |
| FDKF-68 | Fo15:Di75:KF10 | 5 | 1350 | l |
| FDKF-79 | | 7.5 | 1300 | l + fo |

**Table 1** contd.

| Sample | Starting composition, wt% | Duration, h | T °C | Phase composition of run products |
|---|---|---|---|---|
| 1 | 2 | 3 | 4 | 5 |
| FDKF-56 | | 6.5 | 1250 | l + fo + di |
| FDKF-25 | | 55 | 1200 | l + fo + di |
| FDKF-9 | | 75 | 1150 | l + fo + di + phl |
| FDKF-40 | | 60 | 1100 | l + fo + di + phl |
| FDKF-101 | | 18 | 1050 | l + fo + di + phl + ? |
| FDKF-69 | Fo55:Di25:KF20 | 5 | 1350 | l + fo |
| FDKF-80 | | 7.5 | 1300 | l + fo |
| FDKF-57 | | 6.5 | 1250 | l + fo + phl |
| FDKF-26 | | 55 | 1200 | l + fo + phl |
| FDKF-10 | | 75 | 1150 | l + fo + phl + di |
| FDKF-41 | | 60 | 1100 | l + fo + phl + di |
| FDKF-102 | | 18 | 1050 | l + fo + phl + di + cu |
| FDKF-90 | Fo40:Di40:KF20 | 7 | 1216 | l + fo + phl |
| FDKF-114 | | 7 | 1130 | l + fo + phl + di |
| FDKF-70 | Fo30:Di50:KF20 | 5 | 1350 | l + fo |
| FDKF-81 | | 7.5 | 1300 | l + fo |
| FDKF-58 | | 6.5 | 1250 | l + fo |
| FDKF-27 | | 55 | 1200 | l + fo |
| FDKF-150 | | 24 | 1190 | l + fo + phl |
| FDKF-147 | | 5 | 1170 | l + fo + di + phl + lc |
| FDKF-11 | | 75 | 1150 | l + fo + di + phl |
| FDKF-42 | | 60 | 1100 | l + fo + di + phl + ak |
| FDKF-103 | | 18 | 1050 | fo + di + phl + ak + cu |
| FDKF-91 | Fo15:Di65:KF20 | 7 | 1216 | l + fo |
| FDKF-151 | | 24 | 1190 | l + fo + di |
| FDKF-148 | | 5 | 1170 | l + di + lc + phl |
| FDKF-115 | | 7 | 1130 | l + di + lc + phl |
| FDKF-104 | | 18 | 1050 | l + di + lc + phl |
| FDKF-152 | Fo10:Di60:KF30 | 24 | 1190 | l + lc + phl |
| FDKF-149 | | 5 | 1170 | l + lc + phl + di |
| FDKF-116 | | 7 | 1130 | l + lc + phl + di |
| FDKF-71 | Fo40:Di20:KF40 | 5 | 1350 | l |
| FDKF-82 | | 7.5 | 1300 | l + fo + phl |
| FDKF-59 | | 6.5 | 1250 | l + fo + phl |
| FDKF-28 | | 55 | 1200 | l + fo + phl |
| FDKF-12 | | 75 | 1150 | l + fo + phl + sp |
| FDKF-43 | | 60 | 1100 | fo + phl + di + ak + traces lc |
| FDKF-105 | | 18 | 1050 | fo + phl + di + ak + cu + traces lc |
| FDKF-92 | Fo30:Di30:KF40 | 7 | 1216 | l + phl |
| FDKF-117 | | 7 | 1130 | l + phl + lc + di |
| FDKF-106 | | 18 | 1050 | l + phl + lc + di + cu |
| FDKF-125 | | 53 | 993 | l + phl + lc + di + cu |
| FDKF-131 | | 50 | 950 | phl + lc + di + ak + cu |
| FDKF-83 | Fo20:Di40:KF40 | 7.5 | 1300 | l |
| FDKF-60 | | 6.5 | 1250 | l + phl |
| FDKF-29 | | 55 | 1200 | l + phl + lc + traces fo |
| FDKF-13 | | 75 | 1150 | l + phl + lc |
| FDKF-118 | | 7 | 1130 | l + phl + lc |
| FDKF-44 | | 60 | 1100 | l + phl + lc + di |
| FDKF-93 | Fo10:Di50:KF40 | 7 | 1216 | l + lc + phl |
| FDKF-119 | | 7 | 1130 | l + lc + phl |
| FDKF-84 | Fo20:Di20:KF60 | 7.5 | 1300 | l |
| FDKF-61 | | 6.5 | 1250 | l + phl |
| FDKF-30 | | 55 | 1200 | l + phl |
| FDKF-14 | | 75 | 1150 | l + phl |
| FDKF-45 | | 60 | 1100 | l + phl + lc |
| FDKF-107 | | 18 | 1050 | l + phl + lc |
| FDKF-126 | | 53 | 993 | l + phl + lc |
| FDKF-62 | Fo10:Di10:KF80 | 6.5 | 1250 | l |
| FDKF-94 | | 7 | 1216 | $l_s + l_f$ |
| FDKF-31 | | 55 | 1200 | $l_s + l_f$ + phl |
| FDKF-15 | | 75 | 1150 | $l_s + l_f$ + phl |
| FDKF-46 | | 60 | 1100 | $l_s + l_f$ + phl |
| FDKF-108 | | 18 | 1050 | $l_s + l_f$ + phl |
| FDKF-127 | | 53 | 993 | $l_s + l_f$ + phl |
| FDKF-135 | | 50 | 950 | $l_s + l_f$ + phl |

**Table 1** contd.

| Sample | Starting composition, wt% | Duration, h | T °C | Phase composition of run products |
|---|---|---|---|---|
| 1 | 2 | 3 | 4 | 5 |
| Akermanite – F-phlogopite join | | | | |
| AP-46 | Ak80:Phl20 | 6 | 1350 | l |
| AP-31 | | 6 | 1300 | l + ak |
| AP-19 | | 4 | 1250 | l + ak + fo |
| AP-13 | | 9 | 1200 | l + ak + fo |
| AP-1 | | 5 | 1170 | l + ak + fo |
| AP-62 | | 9 | 1150 | l + ak + fo |
| AP-37 | | 7 | 1130 | l + ak + fo + di |
| AP-7 | | 24 | 1100 | l + ak + fo + di + phl |
| AP-69 | | 32 | 1075 | l + ak + fo + di + phl |
| AP-25 | | 70 | 1050 | ak + fo + di + phl + cu |
| AP-32 | Ak70:Phl30 | 6 | 1300 | l |
| AP-20 | | 4 | 1250 | l + fo + ak |
| AP-14 | | 9 | 1200 | l + fo + ak |
| AP-2 | | 5 | 1170 | l + fo + ak |
| AP-63 | | 9 | 1150 | l + fo + ak |
| AP-38 | | 7 | 1130 | l + fo + ak + di |
| AP-8 | | 24 | 1100 | l + fo + ak + di + phl |
| AP-70 | | 32 | 1075 | l + fo + ak + di + phl |
| AP-26 | | 70 | 1050 | fo + ak + phl + di + cu |
| AP-48 | Ak60:Phl40 | 6 | 1350 | l |
| AP-33 | | 6 | 1300 | l + fo |
| AP-21 | | 4 | 1250 | l + fo |
| AP-52 | | 5.5 | 1225 | l + fo |
| AP-15 | | 9 | 1200 | l + fo + ak |
| AP-3 | | 5 | 1170 | l + fo + ak |
| AP-64 | | 9 | 1150 | l + fo + ak + lc |
| AP-43 | | 7 | 1130 | l + fo + ak + lc + di |
| AP-9 | | 24 | 1100 | l + fo + ak + lc + di + phl |
| AP-71 | | 32 | 1075 | l + fo + ak + di + phl |
| AP-27 | | 70 | 1050 | fo + ak + phl + di + cu |
| AP-49 | Ak50:Phl50 | 6 | 1350 | l |
| AP-34 | | 6 | 1300 | l + fo |
| AP-22 | | 4 | 1250 | l + fo |
| AP-16 | | 9 | 1200 | l + fo |
| AP-4 | | 5 | 1170 | l + fo + lc |
| AP-65 | | 9 | 1150 | l + fo + lc + ak |
| AP-44 | | 7 | 1130 | l + fo + lc + ak + di |
| AP-10 | | 24 | 1100 | l + fo + lc + phl + ak + di |
| AP-72 | | 32 | 1075 | l + fo + phl + ak + di |
| AP-28 | | 70 | 1050 | fo + ak + phl + di + cu |
| AP-50 | Ak40:Phl60 | 6 | 1350 | l |
| AP-35 | | 6 | 1300 | l + fo |
| AP-23 | | 4 | 1250 | l + fo |
| AP-53 | | 5.5 | 1225 | l + fo |
| AP-17 | | 9 | 1200 | l + fo + lc |
| AP-5 | | 5 | 1170 | l + fo + lc |
| AP-66 | | 9 | 1150 | l + fo + lc + phl |
| AP-41 | | 7 | 1130 | l + fo + lc + phl |
| AP-11 | | 24 | 1100 | l + fo + traces lc + phl + ak + di |
| AP-73 | | 32 | 1075 | l + fo + phl + ak + di |
| AP-29 | | 70 | 1050 | fo + ak + phl + di + cu |
| AP-75 | Ak20:Phl80 | 5 | 1375 | l |
| AP-67 | | 4 | 1370 | l + fo |
| AP-36 | | 6 | 1300 | l + fo |
| AP-24 | | 4 | 1250 | l + fo + phl |
| AP-54 | | 5.5 | 1225 | l + fo + phl + lc |
| AP-18 | | 9 | 1200 | l + fo + phl + lc |
| AP-6 | | 5 | 1170 | l + fo + phl + lc |
| AP-12 | | 24 | 1100 | l + fo + phl + lc + ak |
| AP-74 | | 32 | 1075 | l + fo + phl + ak |
| AP-30 | | 70 | 1050 | fo + phl + ak + di + cu |
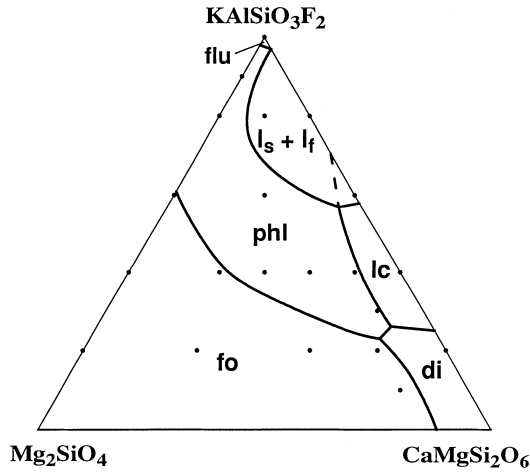
**Fig. 2** Primary phase fields of the $Mg_2SiO_4$ – $CaMgSi_2O_6$ – $KAlSiO_3F_2$ pseudo-ternary join. *Points* indicate positions of reactant mixtures (starting compositions). For abbreviations see the Appendix



**Fig. 4** *T-x* phase diagram of the Diopside – $KAlSiO_3F_2$ pseudo-binary join; data from Table 1

### Akermanite

Early liquidus akermanite forms larger (50–60 μm) tabular crystals. In near-solidus runs melilite occurs as irregular interstitial fillings and can only with difficulty be identified in the microscope.

The chemical composition of melilite in the run products (Table 3) is close to that of pure akermanite. Aluminium and potassium were detected in small amounts (1.36–1.82 wt% $Al_2O_3$ and 0.18–0.85 wt% $K_2O$) and they seem to enter melilite solid solution in the form of K-melilite ($KCaAlSi_2O_7$; K equivalent to sodamelilite) and gehlenite ($Ca_2Al_2SiO_7$) components.

### F-Phlogopite

F-phlogopite usually occurs as hexagonal plates or scales that have a distinctive lustre visible to the naked



**Fig. 3** *T-x* phase diagram of the Akermanite – F-phlogopite pseudo-binary join; data from Table 1
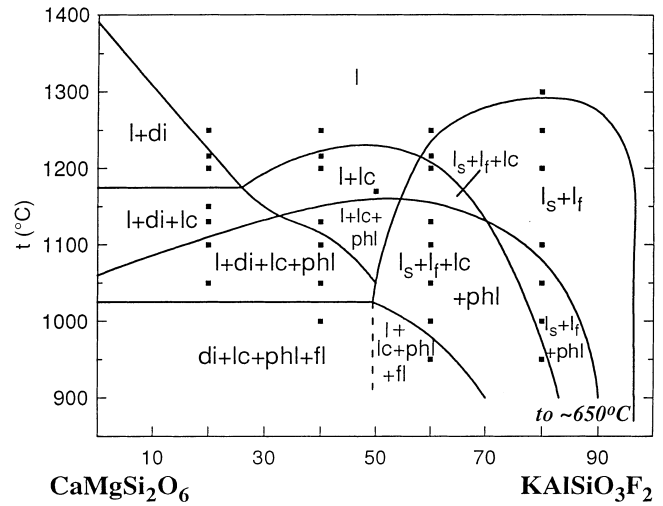
eye in the run products. Small F-phlogopite needles appeared in a few runs and are interpreted to be quench crystals. Representative EMP analyses of F-phlogopite are listed in Table 4. Aluminium is only present in tetrahedral sites of the phlogopite structure. The Al/Si mole values vary (0.196–0.34) and correlate positively to the magnesium content. Thus, it is possible to suggest, that excess silicon in tetrahedral sites (relative to ideal formula) is counterbalanced by vacancies in octahedral sites and the main substitution mechanism for the phlogopite solid solutions is: $Mg^{VI} + 2Al^{IV} = 2Si^{IV} + \square^{VI}$. Similar substitution has been described by Robert (1976) and Melzer and Foley (1996) for synthetic phlogopite in the $SiO_2 - Al_2O_3 - MgO - K_2O - H_2O$ (F) system.

### Spinel

Small amounts of spinel occur in some forsterite-rich runs as well-shaped isotropic octahedral crystals with very high refractive index. A single EMP analysis shows a pure Mg-Al phase ($MgAl_2O_4$). Spinel seems to disappear at lower temperatures due to the reaction with liquid.

### Cuspidine

Cuspidine is a near-solidus and sub-solidus phase which is identified only by EMP. Analyses show that cuspidine contains MgO in essential amounts (2.61–3.36 wt%). The average composition of 14 analyses is: $(Ca_{3.7}Mg_{0.26} K_{0.02})Si_2O_7F_2$.

### Fluorite and other minor phases

Fluorite was detected by XRF analyses and EMP in some sub-solidus leucite-bearing assemblages (see

**Table 2** Representative compositions of clinopyroxene in wt% of oxides and atoms per formula unit (*n* number of analyses)

| Sample | DKF 98 | FDKF 42 | FDKF 148 | FDKF 115 | AP43 | AP9 | AP10 | AP11 | AP29 |
|---|---|---|---|---|---|---|---|---|---|
| n | 3 | 2 | 2 | 2 | 2 | 4 | 4 | 3 | 2 |
| $SiO_2$ | 54.88 | 54.24 | 54.89 | 55.11 | 54.13 | 53.22 | 53.23 | 54.20 | 53.37 |
| $Al_2O_3$ | 0.58 | 0.75 | 0.84 | 0.25 | 1.15 | 2.30 | 2.14 | 1.79 | 2.51 |
| MgO | 19.17 | 19.22 | 20.65 | 20.60 | 19.44 | 18.89 | 18.89 | 18.70 | 18.47 |
| CaO | 26.50 | 25.62 | 24.16 | 24.19 | 26.24 | 26.06 | 25.87 | 25.37 | 25.29 |
| $K_2O$ | 0.09 | 0.09 | 0.01 | 0.01 | 0.07 | 0.10 | 0.06 | 0.08 | 0.09 |
| F | 0.04 | 0.06 | 0.01 | 0.01 | 0.01 | 0.08 | 0.08 | 0.05 | 0.20 |
| Sum | 101.24 | 99.96 | 100.54 | 100.14 | 101.01 | 100.62 | 100.25 | 100.19 | 99.93 |
| Atoms per 6 oxygens | | | | | | | | | |
| Si | 1.96 | 1.96 | 1.96 | 1.98 | 1.94 | 1.92 | 1.92 | 1.95 | 1.93 |
| Al | 0.02 | 0.03 | 0.04 | 0.01 | 0.05 | 0.10 | 0.09 | 0.08 | 0.11 |
| Mg | 1.02 | 1.04 | 1.10 | 1.10 | 1.04 | 1.02 | 1.02 | 1.00 | 1.00 |
| Ca | 1.02 | 0.99 | 0.93 | 0.93 | 1.01 | 1.01 | 1.00 | 0.98 | 0.98 |
| K | 0.00 | 0.00 | 0.00 | 0.00 | 0.00 | 0.01 | 0.00 | 0.00 | 0.00 |
| F | 0.01 | 0.01 | 0.00 | 0.00 | 0.00 | 0.01 | 0.01 | 0.01 | 0.02 |

**Table 3** Compositions of melilite in wt% of oxides and atoms per formula unit (*n* number of analyses)

| Sample | FDKF42 | AP15 | AP43 | AP9 | AP10 | AP11 | AP29 |
|---|---|---|---|---|---|---|---|
| n | 2 | 2 | 7 | 3 | 3 | 3 | 2 |
| $SiO_2$ | 43.51 | 44.22 | 43.57 | 43.65 | 44.04 | 44.44 | 44.01 |
| $Al_2O_3$ | 1.82 | 0.01 | 1.38 | 1.36 | 1.57 | 1.51 | 1.61 |
| MgO | 13.73 | 15.17 | 13.93 | 13.91 | 13.69 | 13.66 | 13.49 |
| CaO | 40.15 | 41.96 | 40.67 | 40.72 | 40.20 | 39.38 | 39.02 |
| $K_2O$ | 0.68 | 0.18 | 0.62 | 0.76 | 0.70 | 0.59 | 0.85 |
| F | 0.19 | 0.01 | 0.03 | 0.01 | 0.01 | 0.01 | 0.08 |
| Sum | 100.07 | 101.51 | 100.18 | 100.39 | 100.21 | 99.59 | 99.06 |
| Atoms per 7 oxygens | | | | | | | |
| Si | 1.98 | 1.98 | 1.98 | 1.98 | 1.99 | 2.01 | 2.01 |
| Al | 0.10 | 0.00 | 0.07 | 0.07 | 0.08 | 0.08 | 0.09 |
| Mg | 0.93 | 1.01 | 0.94 | 0.94 | 0.92 | 0.92 | 0.92 |
| Ca | 1.96 | 2.02 | 1.98 | 1.98 | 1.95 | 1.91 | 1.91 |
| K | 0.04 | 0.01 | 0.04 | 0.04 | 0.04 | 0.03 | 0.05 |
| F | 0.03 | 0.00 | 0.00 | 0.00 | 0.00 | 0.00 | 0.01 |

Table 1). Its chemical composition is close to pure $CaF_2$, but contains about 1.5 wt% $MgF_2$.

An unidentified anisotropic phase, presumably $K_3AlF_6$, appears on the liquidus of the $KAlSiO_3F_2$ bulk composition at ca. 650 °C. It forms thin elongated crystals, or stubby plates and seems to have high birefringence.

Finally a representative of the humite group (F-chondrodite ?) was detected by a single EMP analysis in the sub-solidus assemblage of the Forsterite – $KAlSiO_3F_2$ join (see Table 1) and this phase may be present in trace amounts.

## Topology of phase equilibria

### Components and the phase rule

In a strict sense the studied joins are pseudo-binary and pseudo-ternary sub-systems of the seven-component Si – Al – Mg – Ca – K – O – F system. Nevertheless, the following assumptions allow to reduce the number of components and to use three-dimension coordinates of the kalsilite-based normative tetrahedron (Fig. 1) for the graphic representation of phase equilibria and for the comparison to the relations established in volatile-free systems.

Firstly, the mass proportion of vapour, as mentioned above, seems to be negligible and the system may be treated as condensed. Thus, it is possible to present the components in the conventional oxide form and exclude the fluorine component ($2F^- = O^{2-}$). In effect, variations in F-O substitution and fluorine content of the phases will not show, and some F-bearing phases plot in the same positions as the corresponding F-free ones (for example, $Ca_4Si_2O_7F_2$ (cuspidine) and $Ca_2SiO_4$ (larnite). But the vast majority of phases differ in components other than F and O and retain a unique position within the tetrahedron.

Secondly, it is possible to combine $Al_2O_3$ and $K_2O$ into a single kalsilite ($KAlSiO_4$) component, because K/Al mole values for all starting compositions are equal to 1. It should, however, be noted that in some phases (such as spinel and in clinopyroxene, melilite and

**Table 4** Representative phlogopite compositions in wt% of oxides and atoms per formula unit (*n* number of analyses)

| Sample | DKF 112 | DKF 37 | FDKF 147 | DKF 121 | FDKF 42 | FDKF 103 | FDKF 148 | FDKF 125 |
|---|---|---|---|---|---|---|---|---|
| *n* | 2 | 2 | 2 | 2 | 2 | 2 | 3 | 2 |
| $SiO_2$ | 44.81 | 41.93 | 43.22 | 48.01 | 43.22 | 44.31 | 42.51 | 42.03 |
| $Al_2O_3$ | 10.05 | 12.06 | 11.24 | 7.98 | 11.53 | 10.32 | 11.69 | 11.62 |
| MgO | 28.32 | 28.50 | 28.62 | 27.63 | 28.68 | 28.13 | 29.12 | 28.45 |
| CaO | 0.18 | 0.11 | 0.15 | 0.01 | 0.15 | 0.17 | 0.09 | 0.42 |
| $K_2O$ | 10.79 | 10.78 | 10.98 | 10.36 | 10.91 | 10.96 | 10.86 | 10.75 |
| F | 8.39 | 8.57 | 8.37 | 8.16 | 8.27 | 8.39 | 8.49 | 8.17 |
| Sum | 98.99 | 98.40 | 99.12 | 98.78 | 99.34 | 98.80 | 99.26 | 98.07 |
| *Atoms per 10 oxygens* | | | | | | | | |
| Si | 3.13 | 2.97 | 3.02 | 3.31 | 3.01 | 3.10 | 2.98 | 2.97 |
| Al | 0.83 | 1.01 | 0.93 | 0.65 | 0.95 | 0.85 | 0.97 | 0.97 |
| Mg | 2.94 | 3.01 | 2.99 | 2.84 | 2.98 | 2.94 | 3.04 | 3.00 |
| Ca | 0.01 | 0.01 | 0.01 | 0.00 | 0.01 | 0.01 | 0.01 | 0.03 |
| K | 0.96 | 0.97 | 0.98 | 0.91 | 0.97 | 0.98 | 0.97 | 0.97 |
| F | 1.85 | 1.92 | 1.85 | 1.78 | 1.82 | 1.86 | 1.88 | 1.83 |

**Table 4** (continued)

| Sample | FDKF106 | FDKF 117 | FDKF92 | AP9 | AP10 | AP11 | AP29 |
|---|---|---|---|---|---|---|---|
| *n* | 2 | 2 | 2 | 3 | 3 | 3 | 2 |
| $SiO_2$ | 42.25 | 42.67 | 42.46 | 41.78 | 41.81 | 43.17 | 42.88 |
| $Al_2O_3$ | 11.02 | 12.13 | 11.78 | 12.08 | 11.99 | 12.14 | 12.01 |
| MgO | 28.11 | 28.85 | 28.76 | 28.93 | 29.03 | 28.42 | 28.36 |
| CaO | 1.44 | 0.09 | 0.14 | 0.17 | 0.15 | 0.21 | 0.23 |
| $K_2O$ | 10.55 | 10.84 | 10.94 | 10.88 | 10.60 | 10.95 | 10.99 |
| F | 8.69 | 8.11 | 8.04 | 8.35 | 8.40 | 8.41 | 8.47 |
| Sum | 98.47 | 99.32 | 98.78 | 98.76 | 98.52 | 99.85 | 99.46 |
| *Atoms per 10 oxygens* | | | | | | | |
| Si | 3.01 | 2.96 | 2.97 | 2.94 | 2.95 | 3.00 | 3.00 |
| Al | 0.93 | 0.99 | 0.97 | 1.00 | 1.00 | 0.99 | 0.99 |
| Mg | 2.98 | 2.99 | 3.00 | 3.04 | 3.05 | 2.94 | 2.95 |
| Ca | 0.11 | 0.01 | 0.01 | 0.01 | 0.01 | 0.02 | 0.02 |
| K | 0.96 | 0.96 | 0.98 | 0.98 | 0.95 | 0.97 | 0.98 |
| F | 1.96 | 1.78 | 1.78 | 1.86 | 1.88 | 1.85 | 1.87 |

phlogopite solid solutions) $K_2O$ and $Al_2O_3$ tend to behave as independent components. However, the variations in K/Al values during crystallisation are minor and can be neglected.

Data listed in Table 1 show that the number of equilibrium condensed phases (solids and liquids) on the joins at any given temperature never exceeds six. As discussed below, associations of six condensed phases are observed in narrow temperature intervals and they are very close to invariant isobaric equilibria. Thus, phase rule considerations suggest five effective components, and if vapour phase and variations in K/Al values are ignored, main phases and equilibria may be presented in the coordinates of kalsilite-based normative tetrahedron (Fig. 1).

## Thermal barriers

Yoder (1986) has previously shown that phlogopite takes part in a number of heteromorphic relationships and a pattern of tie-lines and sub-tetrahedra within the kalsilite-normative tetrahedron changes drastically when phlogopite stability is achieved. Important features of the volatile-free, and consequently phlogopite-absent, system (Fig. 1a), are thermal barriers close to the kalsilite-forsterite-akermanite (ks-fo-ak) and kalsilite-leucite-akermanite (ks-lc-ak) planes that separate the forsterite-saturated compositions from the highly larnite normative part of the system. In the volatile-free system silica-undersaturated compositions evolve through the fo-mo-ak-ks invariant reaction point further to the fo-ak-lc-ks eutectic (Yoder 1986). The evolution of more silica-rich, but still undersaturated compositions to the right of the fo-ak-lc thermal barrier (Fig. 1a) terminates at the fo-ak-lc-di eutectic (see flow sheet for dry kalsilite-based normative tetrahedron presented by Yoder 1986). The stability of the F-phlogopite – cuspidine assemblage in the F-doped system breaks the ks-fo-ak thermal barrier and permits the liquid to evolve towards highly larnite normative residuals. Pure OH-analogue of cuspidine (custerite) does not appear to exist as a stable compound (Van Valkenburg and Rynders 1958). Similar to the F-doped system, the formation of OH-phlogopite and stabilisation of the phlogopite-monticellite association under $H_2O$-pressure result in the breakdown of the

ks-fo-ak thermal barrier. However, in the hydrated kalsilite-based tetrahedron no tie-line appears to connect phlogopite to the larnite apex (Yoder 1986).

## Sub-solidus assemblages

All batch compositions on the Akermanite – F-phlogopite join crystallise into five-phase ak + phl + fo + di + cu sub-solidus assemblage (Table 1 and Fig. 3). The join is situated between three stable sub-tetrahedra in the F-doped normative tetrahedron (Fig. 1b) and all five phases of the sub-tetrahedra are present in sub-solidus (please notice that the join in fact is a part of the seven-component system).

The Forsterite – Diopside – $KAlSiO_3F_2$ plane cuts across the Akermanite – F-phlogopite join (see Fig. 1b) and thus the same five-phase sub-solidus assemblage is the final assemblage for many $Mg_2SiO_4$ – $CaMgSi_2O_6$ – $KAlSiO_3F_2$ mixtures (see Table 1 and Fig. 2). But for the pseudo-ternary join this sub-solidus five-phase association is not unique and several other sub-solidus assemblages have been found on the join (Table 1). They include: phl + lc + di + ak + cu five-phase association (sample FDKF-131 in Table 1) and four-phase assemblage: di + lc + phl + fl which is present on the Diopside – $KAlSiO_3F_2$ border join (Fig. 4) and in adjacent forsterite-bearing starting compositions. Different sub-solidus assemblages within an isobaric join require thermal barriers, or reaction relations to be involved and this may be valid for the studied joins.

Six-phase isobaric equilibria with forsterite are plotted in Fig. 5 as a fragment of a flow sheet in coordinates of the $KAlSiO_4$ – $Mg_2SiO_4$ – $Ca_2SiO_4$ – $SiO_2$ – F system.

## Reactions

The most important topological feature for the forsterite-bearing liquidus relationships (Fig. 5) is the six-phase l + fo + lc + di + ak + phl reaction "point" in which forsterite and leucite react with F-bearing melt to produce phlogopite:

$$fo + lc + l = phl \qquad (1)$$

and the reaction proceeds until either forsterite, or leucite is completely consumed. The six-phase assemblage: l + fo + lc + di + ak + phl has been found at 1100 °C in three batch compositions in the central part of the Akermanite – F-phlogopite join. On this join leucite is the phase to react-out. As the system in fact is a seven-component system (potassium and aluminium are in a strict sense independent components) the six-phase reaction assemblage is not an invariant point, but a reaction over a temperature range of about 30 °C. Traces of leucite are often preserved at temperatures below the reaction interval, as resorbed solid inclusions in large akermanite crystals and may be considered metastable,
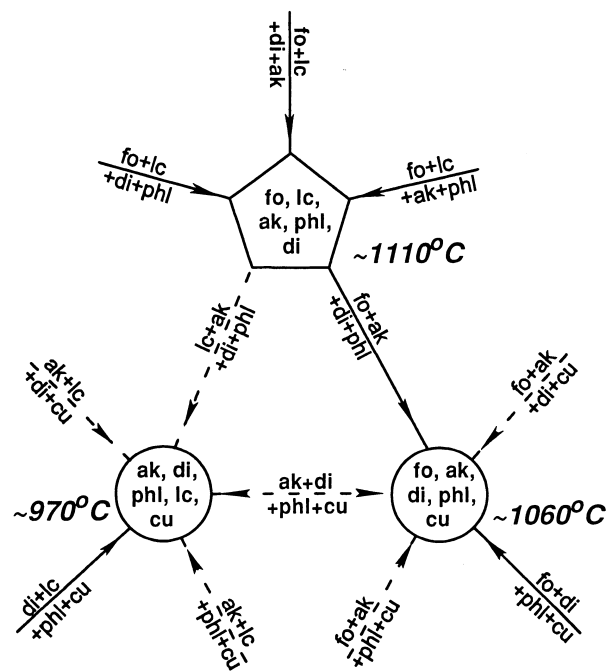


**Fig. 5** Forsterite-saturated, low-silica part of a flow sheet for the $Mg_2SiO_4$ – $Ca_2SiO_4$ – $KAlSiO_4$ – $SiO_2$ – F system at atmospheric pressure showing the six-phase invariant reaction point (*pentagon*) and two eutectics (*circles*). Experimentally determined invariant points and monovariant equilibria are shown in *solid lines*. For abbreviations see the Appendix

because the host effectively protects the remnants of leucite from the liquid and further resorbtion.

The reaction of forsterite and leucite with the F-bearing liquid takes place not only at the reaction "point". For some batch compositions it may start (and end) at higher temperatures along the three peritectic lines leading to the reaction point (see Fig. 5). For example, the resorbtion of leucite on the Akermanite – F-phlogopite join is observed to occur in equilibrium with forsterite, akermanite and diopside before phlogopite appears on the liquidus (Fig. 6). There are also batch compositions, e.g. Fo15:Di65:KF20 in which forsterite is consumed at 1175 °C while leucite remains on the liquidus and in the solidus assemblage together with diopside, leucite and phlogopite (see Table 1). Below the temperature of the l + fo + lc + ak + phl + di reaction point the system may evolve either to the l + ak + di + phl + lc + cu or to the l + fo + ak + di + phl + cu eutectics (Fig. 5) depending on which solid phase (forsterite, or leucite) is consumed first.

Other six-phase reaction points appear to be present in the forsterite-absent parts of the system. Six-phase equilibrium of di, lc, phl and fl with two immiscible liquids (silicate and fluoride) seems to exist close to the Diopside – $KAlSiO_3F_2$ border join at about 1050 °C (Fig. 4). It suggests a major homogeneous exchange reaction between species in the liquid:

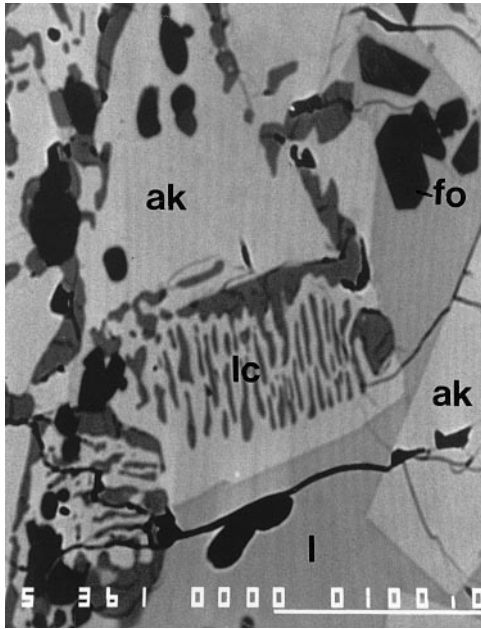$$CaMgSi_2O_6 + 2KAlSiO_3F_2 = CaF_2 + MgF_2 + 2KAlSi_2O_6 \qquad (2)$$
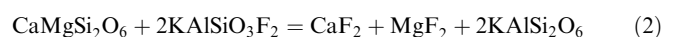
**Fig. 6** Back-scatter electron image of the sample AP-43 showing leucite resorbtion in equilibrium with akermanite (*large*, *light euhedral crystals*), forsterite (*dark*, *small euhedral crystals*) and the melt (*light-grey regions*)

Phase equilibria on the Diopside – $KAlSiO_3F_2$ join imply that the right-hand assemblage of species is stable in the melt. In the presence of crystalline leucite and fluorite activities of $KAlSi_2O_6$ and $CaF_2$ components in the liquid approach 1. Thus, diopside can crystallise only from F-poor compositions where the $CaMgSi_2O_6$ component is in excess of reaction (2). Forsterite-free compositions that yield diopside crystallise completely at about 1030 °C to di + lc + phl + fl sub-solidus assemblage (see Table 1 and Fig. 4). Solidus temperatures for the F-rich part of the join from which diopside is absent are very low. The experimental data for this part of the system is insufficient for detailed discussions of topology.

## Chemical evolution of the liquid

Electron microprobe analyses of quenched melts (glasses) in the charges on the studied joins provide direct information on the evolution of the coexisting melts. Thermal barriers, discussed in the previous section, result in different trends of melt evolution. Not all the numerous samples listed in Table 1 were studied by EMP. We have focused on the melts in equilibrium with the phase assemblages typical for igneous rocks and paid special attention to phlogopite-bearing assemblages of ultramafic alkaline complexes. Chemical compositions of representative glasses saturated with three or more crystalline phases are listed in Table 5.

## Larnite-normative trend

For all studied batch compositions outside the silicate melt – F-melt immiscibility field MgO and possibly $SiO_2$ contents in the melts decrease and CaO content increases with falling temperature, while $Al_2O_3$ and $K_2O$ concentrations show no significant variation. As a result, the evolved compositions of the residual melts are extremely larnite normative (Table 6).

The larnite-normative melt evolution is illustrated by three typical batch compositions in which forsterite is the first liquidus phase (Figs. 7 and 8). Weight proportions of the phases (Fig. 7) were calculated using mass-balance equations based on EMP analyses of the run products. Common features of all three batch compositions are a strong decrease in proportion of the melt and a rapid growth of phlogopite at the expense of the melt, leucite and forsterite below the temperature of the phlogopite-in reaction (Eq. 1). For the Ak50:Phl50 batch composition the reaction takes place at the six-phase reaction point (see the previous section and the flow sheet in Fig. 5.), but for the other two compositions the reaction occurs at higher temperatures along the l + fo + lc + di + phl peritectic "line". The compositions Ak50:Phl50 and Fo30:Di50:KF20 represent the case where leucite is consumed completely in the reaction and forsterite remains, although in smaller quantities, in the assemblage until total crystallisation. For the Fo15: Di65:KF20 composition, on the contrary, forsterite is the phase to react out, and leucite is preserved in the sub-solidus. The latter batch composition differs from the other two by having fluorite in the sub-solidus assemblage instead of cuspidine.

The evolution of the melt in the three batch compositions is shown in Fig. 8 as concentrations of major components versus temperature and shows the effect of the phlogopite-in reaction. As crystallisation proceeds below the reaction temperature, $SiO_2$, $K_2O$ and $Al_2O_3$ concentrations in the melt decrease, while CaO and F contents increase. The MgO content of the liquid decreases steadily within the whole crystallisation range and is not significantly affected by the reaction. Increase in CaO content of the liquid below the phlogopite-in reaction temperature is obviously related to intense phlogopite crystallisation, because F-phlogopite is rich in all the components except CaO (see Table 4). It should be noted that even akermanite crystallisation does not prevent the growth in CaO (e.g. batch composition Ak50:Phl50, Fig. 8). If leucite is preserved in the liquidus phase assemblage (Fo15:Di65:KF20 batch composition), fluorine initially introduced into the system in the form of the $KAlSiO_3F_2$ component accumulates in the residual melt in greater quantities (Fig. 8, see also increase in Fl norm in Table 6).

The compositions of residual melts for Ak50:Phl50 and Fo30:Di50:KF20 starting mixtures at 1100 °C are very similar (samples AP10 and FDKF42 in Table 5). The CIPW norms show that all residual melts have extremely high normative larnite (Table 6). The norms in

**Table 5** Selected compositions of glasses saturated in three or more crystal phases. Standard deviations are in brackets (*n* number of analyses)

| Sample | *T* °C | *n* | Phases in equilibrium | Composition, wt% | | | | | | |
|---|---|---|---|---|---|---|---|---|---|---|
| | | | | $SiO_2$ | $Al_2O_3$ | MgO | CaO | $K_2O$ | F | Sum |
| FDKF 41 | 1100 | 3 | fo + phl + di | 41.19 (1.82) | 8.42 (0.48) | 12.53 (0.64) | 26.54 (0.38) | 4.65 (0.16) | 6.34 (0.18) | 96.99 |
| FDKF 148 | 1170 | 5 | di + phl + lc | 47.95 (0.14) | 6.09 (0.18) | 16.09 (0.18) | 20.32 (0.40) | 5.45 (0.08) | 5.42 (0.18) | 99.04 |
| FDKF 115 | 1130 | 4 | di + phl + lc | 42.19 (0.46) | 4.86 (0.17) | 13.34 (0.22) | 28.74 (0.10) | 3.72 (0.07) | 9.53 (0.33) | 98.37 |
| FDKF 117 | 1130 | 3 | di + phl + lc | 41.56 (0.10) | 4.59 (0.22) | 13.23 (0.14) | 30.95 (0.19) | 4.59 (0.16) | 7.08 (0.18) | 99.02 |
| DKF 37 | 1100 | 7 | di + phl + lc | 39.13 (0.67) | 13.52 (0.24) | 11.60 (0.34) | 29.04 (0.34) | 3.43 (0.11) | 4.83 (0.28) | 99.52 |
| DKF 98 | 1050 | 6 | di + phl + lc | 35.41 (0.27) | 2.37 (0.16) | 11.75 (0.24) | 40.01 (0.34) | 1.54 (0.11) | 16.94 (0.24) | 100.89 |
| FDKF 104 | 1050 | 5 | di + phl + lc | 39.14 (0.42) | 4.69 (0.16) | 8.85 (0.10) | 35.80 (0.57) | 3.53 (0.04) | 12.80 (0.33) | 99.42 |
| FDKF 125 | 993 | 2 | di + phl + lc + cu | 37.74 (1.48) | 6.59 (0.66) | 18.00 (0.69) | 25.29 (1.95) | 6.20 (0.37) | 9.12 (0.11) | 99.10 |
| DKF 133 | 950 | 4 | phl + lc + fl | 53.25 (0.27) | 23.62 (0.28) | 0.04 (0.03) | 0.19 (0.14) | 11.15 (0.65) | 12.49 (0.55) | 100.73 |
| FDKF 147 | 1170 | 7 | fo + phl + di + lc | 45.48 (0.38) | 5.99 (0.13) | 16.68 (0.36) | 22.03 (0.55) | 5.15 (0.24) | 5.72 (0.29) | 98.64 |
| FDKF 102 | 1050 | 2 | fo + phl + di + cu | 46.65 (1.76) | 11.91 (0.50) | 6.21 (0.33) | 21.85 (1.27) | 7.04 (0.43) | 7.43 (0.67) | 97.97 |
| AP43 | 1130 | 7 | fo + ak + lc + di | 41.87 (0.17) | 5.28 (0.14) | 15.02 (0.56) | 28.63 (1.17) | 5.43 (0.13) | 6.04 (0.18) | 99.73 |
| AP44 | 1130 | 3 | fo + ak + di + lc | 41.63 (0.24) | 5.61 (0.15) | 14.54 (0.29) | 28.69 (0.24) | 5.18 (0.19) | 5.92 (0.12) | 99.08 |
| FDKF 42 | 1100 | 3 | fo + ak + phl + di | 41.59 (0.40) | 4.97 (0.42) | 13.73 (0.24) | 27.7 (0.49) | 5.94 (0.18) | 6.5 (0.39) | 97.69 |
| AP11 | 1100 | 3 | fo + ak + phl + di | 40.65 (0.41) | 3.48 (0.07) | 15.21 (0.21) | 29.32 (0.23) | 6.17 (0.13) | 7.79 (0.02) | 99.34 |
| AP9 | 1100 | 5 | fo + ak + lc + di + phl | 40.30 (0.40) | 3.47 (0.42) | 14.91 (0.24) | 28.90 (0.49) | 6.70 (0.18) | 7.78 (0.39) | 98.78 |
| AP10 | 1100 | 6 | fo + ak + lc + di + phl | 40.44 (0.52) | 3.72 (0.21) | 14.43 (0.24) | 28.24 (0.56) | 6.95 (0.25) | 7.51 (0.16) | 98.13 |

**Table 6** CIPW norms of glasses (quenched liquids) plotted in Figs. 7 and 8. Abbreviations for normative components are listed in the Appendix

| Sample | *T* °C | Phases in equilibrium | Normative compositions of glasses, wt% | | | | | | | |
|---|---|---|---|---|---|---|---|---|---|---|
| | | | Fl | Or | Lc | An | KS | Di | Fo | La |
| Fo30:Di50:KF20 | | | | | | | | | | |
| Starting batch composition | | | 8.67 | 15.49 | 12.07 | | | 25.95 | 37.81 | |
| FDKF70 | 1350 | fo | 7.74 | 17.75 | 9.38 | 0.76 | | 33.06 | 31.31 | |
| FDKF127 | 1200 | fo | 9.53 | 21.45 | 11.56 | 1.50 | | 38.88 | 17.09 | |
| FDKF147 | 1170 | fo + di + phl + lc | 11.91 | | 24.19 | 1.15 | | 44.81 | 14.96 | 2.98 |
| FDKF42 | 1100 | fo + di + phl + ak | 13.67 | | 21.78 | | 3.14 | 30.33 | 14.67 | 16.40 |
| Fo15:Di65:KF20 | | | | | | | | | | |
| Starting batch composition | | | 8.67 | 15.49 | 12.08 | | | 40.95 | 22.81 | |
| FDKF91 | 1220 | fo | 7.93 | 16.76 | 10.58 | 0.99 | | 48.75 | 15.00 | |
| FDKF151 | 1190 | fo + di | 9.78 | 25.65 | 9.79 | 1.55 | | 37.80 | 15.44 | |
| FDKF148 | 1170 | lc + di + phl | 11.24 | 10.27 | 17.44 | 0.53 | | 47.63 | 12.88 | |
| FDKF115 | 1130 | lc + di + phl | 19.91 | | 17.52 | 2.31 | | 51.88 | 6.82 | 1.57 |
| FDKF104 | 1050 | lc + di + phl | 26.59 | | 16.54 | 2.40 | | 48.07 | | 6.40 |
| Ak50:Phl50 | | | | | | | | | | |
| Starting batch composition | | | 9.27 | | 25.91 | | | 19.85 | 31.50 | 13.47 |
| AP22 | 1250 | fo | 8.09 | | 27.86 | | 0.05 | 23.15 | 23.54 | 17.31 |
| AP4 | 1170 | fo + lc | 9.18 | | 27.51 | 0.44 | | 26.01 | 18.23 | 18.63 |
| AP44 | 1130 | fo + lc + ak + di | 12.28 | | 24.23 | | | 25.06 | 17.47 | 20.96 |
| AP10 | 1100 | fo + lc + ak + di + phl | 15.73 | | 16.23 | | 8.15 | 26.61 | 17.02 | 16.27 |
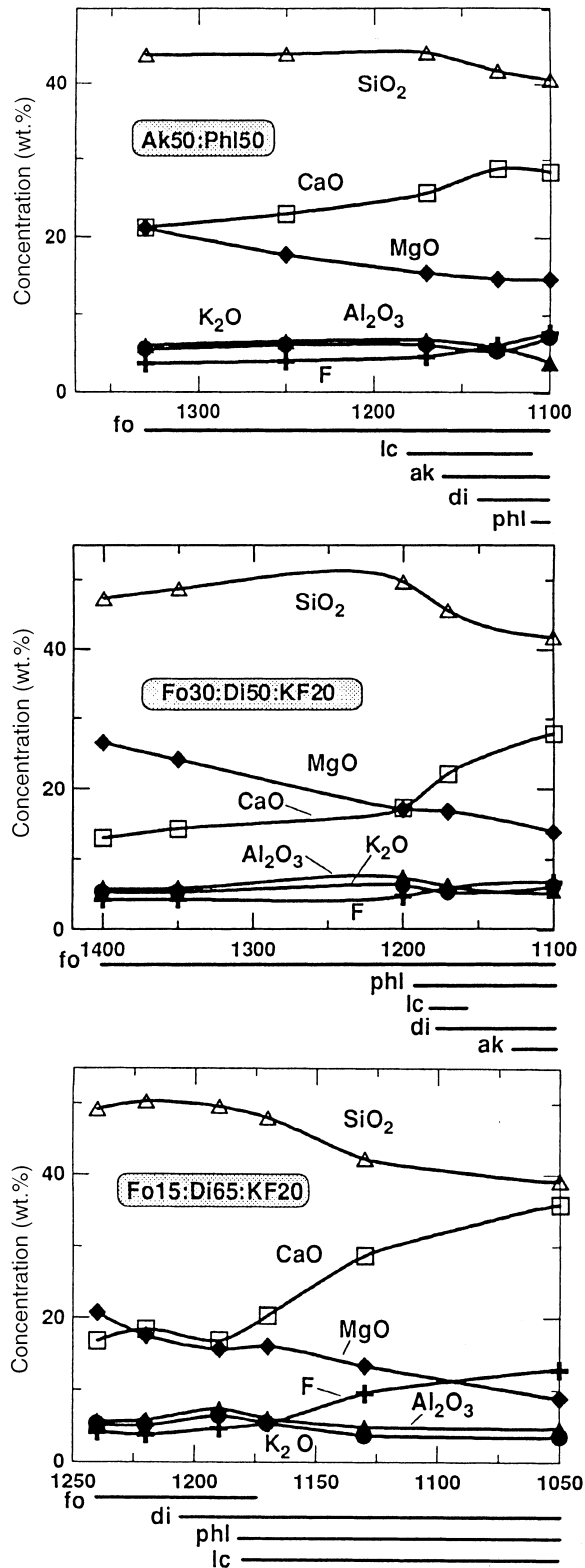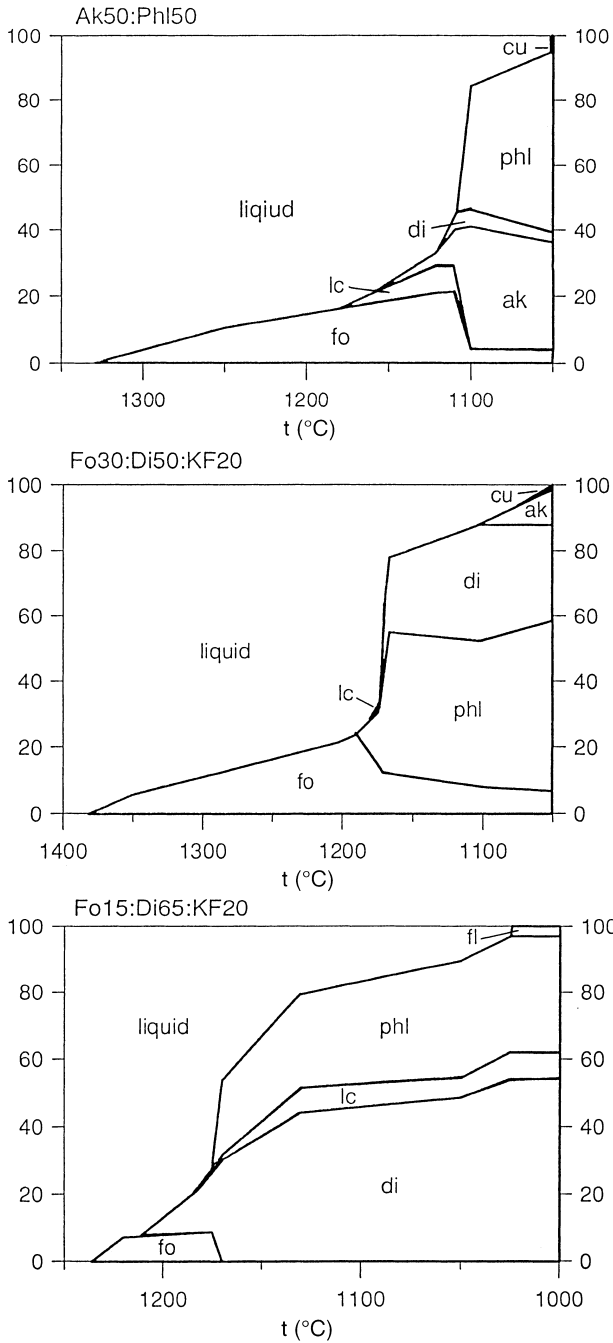
**Fig. 7** Proportions of phases (in wt%) versus temperature for three representative batch compositions. The starting compositions (in wt%) are indicated *above* the plots. Phase proportions are calculated using mass-balance equations and EMP analyses of coexisting phases

Table 6 demonstrate that batch compositions Fo30:Di50:KF20 and Fo15:Di65:KF20 are examples of melanephelinitic compositions which initially are not larnite normative, but evolve to highly larnite normative (melilitite) residuals due to phlogopite crystallisation. In other words, they illustrate fractionation across the thermal barrier of the dry system to larnite-normative melilititic compositions under volatile pressure in accordance with the suggestions of Nielsen (1994) and Nielsen et al. (1997).



**Fig. 8** Compositions of the remaining liquids (in wt% of oxides) versus temperature for the same batch compositions as in Fig. 7. *Lines below* the plots show crystallisation intervals for liquidus phases. For abbreviations see the Appendix

Homogeneous exchange reaction (2) seems to be a limiting factor for the larnite-normative trend of melt

evolution. In the F-rich part of the $Mg_2SiO_4$ – $CaMgSi_2O_6$ – $KAlSiO_3F_2$ join where the $KAlSiO_3F_2$ component is in excess and neither diopside, nor forsterite are stable other trends are observed. For example, low-temperature residual liquids in equilibrium with leucite, phlogopite and fluorite are very Mg and Ca poor, $SiO_2$-rich and per-aluminous (sample DKF-133 in Table 5). Low K/Al mole values of these liquids are believed to result from crystallisation of phlogopite solid solutions with K/Al > 1 (due to the above-mentioned $Mg^{VI}$ + $2Al^{IV}$ = $2Si^{IV}$ + $\Box^{VI}$ substitution). Liquid immiscibility is another phenomenon affecting the liquid evolution in the F-rich part of the system.

### Silicate-fluoride liquid immiscibility

Immiscible fluorine-rich liquid occurs as spherical droplets, 20–100 microns in diameter, in the part of $Mg_2SiO_4$ – $CaMgSi_2O_6$ – $KAlSiO_3F_2$ join adjacent to the $CaMgSi_2O_6$ – $KAlSiO_3F_2$ border (Figs. 2 and 4). When quenched the fluorine-rich melt droplets crystallise to fine-grained aggregates and the conjugate silicate liquid often quenches to turbid, opacified glass. At lower temperatures silicates (leucite and/or phlogopite) start to crystallise in equilibrium with the immiscible liquids (see Table 1). Onset of the fluorite crystallisation together with leucite and phlogopite is a low-temperature limit for the liquid immiscibility (Fig. 4). The immiscibility field is located in a very F rich portion of the $Mg_2SiO_4$ – $CaMgSi_2O_6$ – $KAlSiO_3F_2$ join and is separated from the field of petrologically relevant compositions by the field of F-phlogopite. Thus, silicate–fluoride liquid immiscibility has little importance for applications discussed below. Details of phase equilibria and chemical composition of the immiscible liquids will be presented elsewhere.

### Discussion

The application of the experimental results to natural magmatic systems requires examination of the intrinsic limitations. The simplified experimental system studied excludes major magmatic components such as ferrous and ferric iron, titanium, sodium, phosphorus and some phases common in natural magmatic systems are not present in the run products. It is also clear that the application is restricted to a limited, silica-undersaturated compositional range and low, crustal pressures. It can also be questioned to what extent the fluorine-doped system models the phase equilibria in natural volatile-bearing silicate melts. In general, $H_2O$ rather than F is the main volatile component in natural magmas. Detailed discussion on the effect of the $H_2O$-F ratio on the crystallisation and properties of silicate melts is a broad field beyond the general scope of the study, but some effects are of great importance and outlined below.

### Fluorine and water in silicate melts

Fluorine contents in the experimental batch compositions are much higher than those usually observed in igneous rocks and expected in natural magmatic melts. The F concentrations can only be compared to F concentrations in rare topaz-bearing rhyolites and ongonites with bulk-rock concentrations as high as 2–4.5 wt% (Congdon and Nash 1988; Kovalenko 1973). Melt inclusions in quartz suggest that fluorine content in the evolved silicic melts parental for these rocks may be even higher, up to 5.5 wt% (Carroll and Webster 1994). Very high bulk-rock F concentrations for mantle-derived mafic rocks are found in lamproites (up to 0.76 wt% F, Aoki et al. 1981; Edgar and Charbonneau 1991). These values are 3–4 times higher than the F concentrations in other mafic-ultramafic rocks and 6–8 times greater than in tholeiitic basalts. Thus, it must be expected that the F concentration in the silica-undersaturated mantle-derived magmatic melts is an order of magnitude lower than in the synthetic mixtures.

Water is believed to be the most abundant volatile component in magmas and despite the fact that F and $H_2O$ (OH) play similar roles and generally substitute for each other in crystal structures there are many significant differences in their chemistry. The F-OH exchange influences the stability and physical properties of volatile-bearing crystalline phases and, as previously pointed out, the thermal stability of F-phlogopite significantly exceeds that of the hydroxyl analogue (Munoz 1984). Other F-bearing phases in the studied systems either do not have hydroxyl equivalents, e.g. cuspidine, or the hydrated phases have never been reported to crystallise from $H_2O$-bearing silicate melts.

The solubilities of $H_2O$ and F in silicate melts have recently been reviewed by Carroll and Webster (1994) and McMillan (1994). Despite much controversy it is strongly suggested that fluorine forms complexes in aluminosilicate melts with network modifying cations, such as alkali and alkaline earths (Krigman and Kogarko 1981; Foley et al. 1986). This implies that F enhances the polymerisation of the melt and increases the activity of highly polymerised crystalline phases.

On the other hand, there is a strong evidence in favour of the depolymerising effect of water on the melt structure (McMillan 1994). In polymerised hydrated aluminosilicate melts linkages between tetrahedrally coordinated ions seem to be weakened (if not broken) by attachment of hydrogen to bridging oxygen and this may have important consequences for the crystallisation of the melts in $H_2O$-bearing systems.

Zeng and MacKenzie (1984) showed that $H_2O$ decreases the stability of leucite and that the liquidus field of leucite shrinks dramatically under increasing water pressure. If the relative stabilities of phlogopite and leucite in analogue fluorine-doped and water-bearing systems can be compared it should be expected that both phases are less stable in hydrated systems, but the F-OH substitution may affect leucite stability to a greater

extent than the stability of phlogopite and this may change the topology of phase equilibria.

## Effects of pressure

Akermanite is not stable at high pressure. Its stability field in the anhydrous systems is limited to a maximum pressure of about 15 kbar (Yoder 1986). Melzer and Foley (1996) demonstrated that leucite stability in the $KAlSiO_4 - Mg_2SiO_4 - SiO_2 - F$ system depends on pressure and F content of batch compositions. Leucite was found to disappear from associations of liquidus phases at 10 kbar for 6 wt% F and 18 kbar for 3 wt% F. Neither leucite, nor akermanite are thus expected to be present at high pressures in phase associations of the kalsilite-based tetrahedron. However, instability of melilite and leucite will not prevent melts from evolving towards Ca-rich residuals. As shown above, the key phase for the larnite-normative trend is phlogopite and as long as the association fo + cpx + phl is stable the silica-undersaturated liquids may evolve towards the larnite apex of the normative tetrahedron (Fig. 1b).

Phlogopite liquidi are usually very steep on $P$-$T$ phase diagrams for potassic rocks and in synthetic systems and it seems that pressure above 0.7 kbar has minor effect on the stability of phlogopite.

No compositional data appear to exist for glasses in equilibrium with forsterite, Ca-clinopyroxene and phlogopite in the water-bearing kalsilite normative tetrahedron at high pressure. Modreski and Boettcher (1973) report the composition of a glass on the diopside – phlogopite join (reactant mixture 1:1 by weight) at 1250 °C, 15 kbar, but at this temperature the glass is equilibrated with forsterite and diopside only, while phlogopite was found to crystallise at about 50 °C below. Even though, it is worth noticing that the glass is silica undersaturated and slightly larnite normative (0.9 wt% of normative larnite). Our results suggest that the onset of phlogopite crystallisation would drive the melt towards more larnite-rich compositions.

The topology of phase equilibria in the kalsilite-based normative tetrahedron with stable phlogopite (Fig. 1b) suggests that a plane close to the fo-di-phl join is critical for the larnite-normative melt evolution. Compositions above and to the left of this plane, or divide (Fig. 1b) would evolve towards larnite-normative residuals, whereas more $SiO_2$-rich and CaO-poor compositions below and to the right of the plane will not produce larnite-normative melts during fo + di + phl fractionation. Formation of diopside-enstatite solid solutions and the $Mg^{VI} + 2Al^{IV} = 2Si^{IV} + \square^{VI}$ substitution in phlogopite suggest that the critical plane should lie slightly below the fo-di-phl join. Previously published data on rock-melting experiments (see below) indicate that both trends do occur in natural multicomponent systems.

## Applications

### Evolution of the potassic magmas

The results of the experimental study can be applied to the generation and low-pressure evolution of group II ultrapotassic rocks, or kamafugites (classification introduced by Foley et al. 1987). Bulk compositions of kamafugites with leucite, melilite and phlogopite are characterised by low $SiO_2$ and $Al_2O_3$ and high CaO (Foley 1992; Foley et al. 1987). Kamafugite lavas from East Africa and other localities often contain mica-clinopyroxenite and other phlogopite-bearing xenoliths believed to represent the samples of the highly metasomatized mantle source. This suggests that phlogopite plays a fundamental role for the origin and evolution of kamafugites.

The larnite-normative trend which is observed for the liquid in the F-doped system may help to explain the most distinctive chemical features of kamafugite melts: the $SiO_2$ depletion and the CaO enrichment. Liquidus phase equilibria in the model system suggest that partial melting of compositions in the vicinity of the Phl – Di join in the presence of stable phlogopite will produce silica-undersaturated larnite-normative melts. Melting experiments on a representative mantle-derived phlogopite-clinopyroxenite nodule composition reported by Lloyd et al. (1985) show that the larnite-normative trend is real for multicomponent water-bearing compositions. All partial melts produced in these experiments at 20 and 30 kbar in equilibrium with high-Ca clinopyroxene, phlogopite, ilmenite, apatite, magnetite and forsterite are larnite-normative. A series of isobaric runs at 30 kbar show that the CaO content in melts in equilibrium with phlogopite and clinopyroxene increase, while $SiO_2$ and $K_2O$ concentrations decrease with falling temperature and decreasing degrees of partial melting. This is consistent with the observations in the model system and indicates that larnite-normative partial melts can be buffered by the residual clinopyroxene-phlogopite assemblage in the mantle source.

Natural glasses in upper mantle xenoliths from the volcanics of Gees, West Eifel (Edgar et al. 1989) provide further evidence for the genetic link between phlogopite stability in the mantle source and generation of larnite-normative kamafugite melts. Edgar et al. (1989) studied six xenoliths ranging from harzburgite to mica clinopyroxenite. Glasses in association with phlogopite are larnite normative and differ from those surrounding and enclosed by spinel. All phlogopite related glasses show a strong negative correlation between $SiO_2$ and CaO similar to the phlogopite-saturated glasses in the studied F-doped system.

On the other hand, olivine and augite minettes studied by Esperança and Holloway (1987) and Righter and Carmichael (1996) provide examples of compositions with olivine, clinopyroxene and phlogopite on liquidus, that do not follow the larnite-normative

evolution. The bulk compositions are more silica rich, Ca poor and orthoclase normative and plot below the fo-di-phl join in the kalsilite-based normative tetrahedron (Fig. 1b). Crystallisation of the ol-cpx-phl association from these compositions results in the increase of $SiO_2$ and decrease of CaO contents in the residual melts in agreement with the conclusions presented in the previous section.

## Origin of the plutonic melilite-rich rocks

Phlogopite is abundant not only in potassic mafic silica-undersaturated systems, but also in more common sodium-dominated alkaline associations. Phlogopite accumulations in some ultramafic alkaline intrusions are even subjected to mining, e.g. Kovdor, Kola Peninsula. The experimental results and especially the development of residual melts in phlogopite-bearing systems (Fig. 8) imply that late-stage melilitolites of ultramafic alkaline complexes are low-pressure products of fractional crystallisation of phlogopite-bearing assemblages from a melanephelinitic parental melt. Other hydrous minerals, such as amphiboles, may play a role similar to that of phlogopite and also lead to increasing normative larnite.

The absence of the larnite-normative melt evolution in dry systems and the critical role of hydrous phases may also be illustrated by the experimental study of Gee and Sack (1988). In their experiments with natural melilitite lava compositions no increase in normative larnite in residual melts was observed despite larnite-normative starting compositions. Liquidus assemblages in the experiments of Gee and Sack (1988), however, include leucite, nepheline, clinopyroxene, spinel ± melilite ± olivine, and no phlogopite, which in the present study is shown to be the determining phase for the development towards highly larnite normative residuals in response to the increased volatile pressure.

In conclusion, the development of late-stage melilitolitic melts in ultramafic-alkaline complexes (e.g. Kovdor and Gardiner) is dependent on volatile content and the stability of phlogopite. Closed volatile-rich conditions during fractionation will favour a melilitic and possibly also a carbonatitic evolutionary trend as suggested by Nielsen (1994), whereas degassed and anhydrous conditions would favour developments towards more CaO-poor phonolitic residuals.

## Appendix

Abbreviations for phases:

ak akermanite
cu cuspidine
di diopside
en enstatite
fl fluorite
flu unidentified fluoride phase, presumably $K_3AlF_6$
fo forsterite
hu humite
ks kalsilite
la larnite
lc leucite
$l_f$ fluoride melt
$l_s$ silicate melt
mo monticellite
phl phlogopite
sa sanidine
qz quartz
sp spinel
wo wollastonite

Formulae for components:

Ak $Ca_2MgSi_2O_7$
An $CaAl_2Si_2O_8$
Di $CaMgSi_2O_6$
Fo $Mg_2SiO_4$
Fl $CaF_2$
KF $KAlSiO_3F_2$
KS $K_2Si_2O_5$
La $Ca_2SiO_4$
Lc $KAlSi_2O_6$
Or $KAlSi_3O_8$
Phl $KMg_3AlSi_3O_{10}F_2$
Wo $CaSiO_3$

## References

Aoki K, Ishiwaka K, Kanisawa S (1981) Fluorine geochemistry of basaltic rocks from continental and oceanic regions and petrogenetic applications. Contrib Mineral Petrol 76: 53–59

Carroll MR, Webster JD (1994) Solubilities of sulphur, noble gases, nitrogen, chlorine and fluorine in magmas. In: Carroll MR, Holloway JR (eds) Volatiles in magmas. (Reviews in mineralogy, 30) Mineral Soc Am, Washington, DC, pp 231–280

Congdon RD, Nash WP (1988) High-fluorine rhyolite: an eruptive pegmatite magma at the Honeycomb Hills, Utah. Geology 16: 1018–1021

Edgar AD, Charbonneau HE (1991) Fluorine-bearing phases in lamproites. Mineral Petrol 44: 125–149

Edgar AD, Vukadinovic D (1992) Implications of experimental petrology to the evolution of ultrapotassic rocks. Lithos 28: 205–220

Edgar AD, Lloyd FE, Forsyth DM, Barnett RL (1989) Origin of glass in the upper mantle xenoliths from the quaternary volcanics of Gees, West Eifel, Germany. Contrib Mineral Petrol 103: 277–286

Esperança S, Holloway JR (1987) On the origin of some mica lamprophyres: experimental evidence from a mafic minette. Contrib Mineral Petrol 95: 207–216

Foley S (1992) Petrological characterization of the source components of potassic magmas: geochemical and experimental constraints. Lithos 28: 187–204

Foley SF, Taylor WR, Green DH (1986) The effect of fluorine on phase relationships in the system $KAlSiO_4 - Mg_2SiO_4 - SiO_2$ and the solution mechanism of fluorine in silicate melts. Contrib Mineral Petrol 93: 46–55

Foley SF, Venturelli G, Green DH, Toscani L (1987) The ultrapotassic rocks: characteristics, classification, and constraints for petrogenetic models. Earth-Sci Rev 24: 81–134

Gee LL, Sack RO (1988) Experimental petrology of melilite nephelinites. J Petrol 29: 1233–1255

Gupta AK (1972) The system forsterite – diopside – akermanite – leucite and its significance in the origin of potassium-rich mafic and ultramafic volcanic rocks. Am Mineral 57: 1242–1259

Gupta AK, Green DH (1988) The liquidus surface of the system forsterite-kalsilite-quartz at 28 kbar under dry conditions, in the presence of $H_2O$, and of $CO_2$. Mineral Petrol 39: 163–174

Kovalenko VI (1973) Distribution of fluorine in topaz-bearing quartz keratophyre dike (ongonite) and mobility of fluorine in quartz melts. Geochem Int 10: 41–49

Krigman LD, Kogarko LN (1981) Fluorine in silicate melts and magmas (in Russian). Nauka, Moscow

Kushiro I (1970) Stability of amphibole and phlogopite in the upper mantle. Carnegie Inst Washington Year b 68: 245–247

Lloyd FE, Arima M, Edgar AD (1985) Partial melting of a phlogopite clinopyroxenite from south-west Uganda: an experimental study bearing on the origin of highly potassic continental rift volcanics. Contrib Mineral Petrol 91: 321–329

Luth WC (1967) Studies in the system $KAlSiO_4 - Mg_2SiO_4 - SiO_2 - H_2O$. I. Inferred phase relations and petrologic applications. J Petrol 8: 372–416

McMillan PF (1994) Water solubility and speciation models. In: Carroll MR, Holloway JR (eds) Volatiles in magmas. (Reviews in mineralogy, vol 30). Mineral Soc Am, Washington, DC, pp 131–156

Melzer S, Foley S (1996) Phase relationships in the system $KAlSiO_4 - Mg_2SiO_4 - SiO_2 - F$ and the stability of F-phlogopite at atmospheric pressure, 10 and 18 kbar. Neues Jahrb Mineral Abh 171(1): 1–31

Modreski P, Boettcher AL (1973) Phase relationships of phlogopite in the system $K_2O - MgO - CaO - Al_2O_3 - SiO_2 - H_2O$ to 35 kilobars: a better model for micas in the interior of the Earth. Am J Sci 273: 385–414

Munoz JL (1984) F-OH and Cl-OH exchange in micas with applications to hydrothermal ore deposits. In: Bailey SW (ed) Micas. (Reviews in mineralogy, vol 13). Mineral Soc Am, Washington, DC, pp 469–494

Nielsen TFD (1994) Alkaline dike swarms of the Gardiner complex and the origin of ultramafic alkaline complexes. Geochem Int 31(3): 37–56

Nielsen TFD, Solovova IP, Veksler IV (1997) Parental melts of melilitolite and the origin of alkaline carbonatite: evidence from crystallised melt inclusions, Gardiner complex. Contrib Mineral Petrol 126: 331–344

Pan V, Longhi J (1989) Low pressure liquidus relations in the system $Mg_2SiO_4 - Ca_2SiO_4 - NaAlSiO_4 - SiO_2$. Am J Sci 289: 1–16

Pan V, Longhi J (1990) The system $Mg_2SiO_4 - Ca_2SiO_4 - CaAl_2O_4 - NaAlSiO_4 - SiO_2$. 1. Atmosphere liquidus equilibria of analogs of alkaline mafic lavas. Contrib Mineral Petrol 105: 569–584

Righter K, Carmichael ISE (1996) Phase equilibria of phlogopite lamprophyres from western Mexico: biotite-liquid equilibria and $P$-$T$ estimates for biotite-bearing igneous rocks. Contrib Mineral Petrol 123: 1–21

Robert JL (1976) Phlogopite solid solutions in the system $K_2O - MgO - Al_2O_3 - SiO_2 - H_2O$. Chem Geol 17: 195–212

Schairer JF, Bowen NL (1938) The system leucite – diopside – silica. Am J Sci 35A: 289–309

Shell HR and Ivey KH (1969) Fluorine micas. US Bur Mines Bull 647

Soulard H, Provost A, Boivin P (1992) $CaO - MgO - Al_2O_3 - SiO_2 - Na_2O$ (CMASN) at 1 bar from low to high $Na_2O$ contents: topology of an analogue for alkaline basaltic rocks. Chem Geol 96: 459–477

Van Valkenburg A, Rynders GF (1958) Synthetic cuspidine. Am Mineral 43: 1195–1202

Wendlandt RF (1984) An experimental and theoretical analysis of partial melting in the system $KAlSiO_4 - CaO - MgO - SiO_2 - CO_2$ and applications to the genesis of potassic magmas, carbonatites and kimberlites. In: Kornprobst J (ed) Kimberlites and related rocks. Elsevier, Amsterdam, pp 359–369

Wendlandt RF, Eggler DH (1980a) The origins of potassic magmas. 1. Melting relations in the systems $KAlSiO_4 - Mg_2SiO_4 - SiO_2$ and $KAlSiO_4 - MgO - SiO_2 - CO_2$ to 30 kilobars. Am J Sci 280: 385–420

Wendlandt RF, Eggler DH (1980b) The origins of potassic magmas. 2. Stability of phlogopite in natural spinel lherzolite and in the system $KAlSiO_4 - MgO - SiO_2 - H_2O - CO_2$ at high pressures and high temperatures. Am J Sci 280: 421–458

Yoder HS Jr (1986) Potassium-rich rocks: phase analysis and heteromorphic relations. J Petrol 27: 1215–1228

Zeng RS, MacKenzie WS (1984) Preliminary report on the system $NaAlSiO_4 - KAlSiO_4 - SiO_2 - H_2O$ at $PH_2O = 5$ kbar. Bull Mineral 107: 571–577